Communications on Applied Nonlinear Analysis
ISSN: 1074-133X
Vol 31 No. 3s (2024)

# Behavior of Non-Newtonian Nano-Williamson Fluid Flow Over a Stretching Sheet Filled by Porous Medium: Multiple Slips and Magnetic Field Effects

**B. Chandrasekhar[a,b], M. Chenna Krishna Reddy[c]**

[a] Department of Mathematics, JNTUH College of Engineering, Hyderabad, Telangana Sate, India.

[b] Department of Mathematics, Vardhaman College of Engineering, Hyderabad, Telangana Sate, India.

[c] Department of Mathematics, University College of Science, Osmania University, Hyderabad, Telangana Sate, India.

[*]Corresponding author Email address: *shekmaths10@gmail.com*

***Article History:***

***Received:*** *14-04-2024*

***Revised:*** *20-05-2024*

***Accepted:*** *10-06-2024*

**Abstract:**

The intention of this investigation research work is to study Multiple slip (Velocity slip & Concentration) effects on two-dimensional, steady, electrically conducting, incompressible, laminar, viscous, Williamson-nanofluid flow through a porous medium towards a stretching sheet in the presence of magnetic field and chemical reaction is investigated numerically. In this work, similarity transformations are used to derive a set of non-linear partial differential equations governing the flow. The resultant dimensionless ordinary differential equations which are linear are solved numerically by Runge-Kutta method along with shooting technique. In this work, the profiles for velocity, concentration, and temperature are studied by variations of physical parameters graphically. Also the numerical values of heat and mass transfer rates and skin-friction coefficients are presented in tabular forms with variations of above same parameters. Based on these plots and values the conclusions are given, and the obtained results are tested for their accuracy.

**Keywords**: Chemical reaction; Multiple slips; Porous medium; Stretching sheet; Nanofluid; Williamson fluid; Magnetic field; Runge-Kutta method; Shooting method.

## 1. Introduction:

Multi-slip effects refer to the simultaneous occurrence of multiple slip mechanisms in fluid flows. When considering the flow of nanofluids, which are suspensions of nanoparticles in a base fluid, the presence of nanoparticles introduces additional complexities due to their unique characteristics and interactions with the fluid. Williamson nanofluid is a type of nanofluid that exhibits multi-slip effects. It is named after D.L. Williamson, who proposed a model to describe the viscosity of nanofluids with slip effects. In Williamson nanofluids, the nanoparticles can experience slip at the fluid-solid interface, leading to changes in the overall flow behaviour. The slip effect in nanofluids can be classified into different types, such as thermal slip, diffusive slip, and shear slip. Thermal slip occurs when the temperature gradient at the fluid-solid interface induces a velocity slip. Diffusive slip refers to the slip effect caused by the concentration gradient of nanoparticles. Shear slip arises from the shear stress between the nanoparticles and the fluid, leading to a slip velocity. The presence of multi-slip effects in Williamson nanofluids has several consequences on the flow behaviour. Firstly, the slip effects can significantly alter the velocity profiles and shear stress distribution in the flow. The slip velocities at

the fluid-solid interface can modify the overall flow characteristics and affect the heat transfer performance of the nanofluid. Additionally, the slip effects can influence the effective viscosity of the Williamson nanofluid. The effective viscosity is a key parameter that determines the flow resistance and pumping power requirements. By considering the multi-slip effects, the viscosity of the nanofluid can be accurately predicted, accounting for the slip velocities associated with each slip mechanism. Understanding the multi-slip effects on Williamson nanofluid flows is crucial for various applications, such as heat transfer enhancement, micro-fluidics, and energy systems. Proper modeling and characterization of these effects can provide valuable insights into the behaviour of nanofluids and enable better design and optimization of systems involving nanofluid flows. It's worth noting that the study of multi-slip effects in Williamson nanofluids is an active area of research, and ongoing studies continue to explore the underlying mechanisms and develop improved models to accurately capture these effects. Ahmadi et al. [1] focused on modeling the laminar forced convection of a nanofluid inside a tube with uniform heat flux. Ali et al. [2] explored the thermal slip phenomenon in nanofluid-based systems and discusses its implications on system performance. Aswathy and Philip [3] focused on slip velocity models for nanofluids. Slip velocity refers to the relative velocity between the fluid and solid phases at the solid-liquid interface. Aswathy and Philip [4] discussed the multi-slip effect in nanofluid flow. Multi-slip refers to the presence of different slip mechanisms simultaneously, such as thermal slip and velocity slip. Bhanvase and Chhabra [5] investigated the slip flow heat transfer characteristics of nanofluids in microchannels. Chein et al. [6] focused on the mixed convection flow of Williamson nanofluid through a vertical wavy channel. Ghosh and Das [7] investigated the multi-slip effects on mixed convection flow and heat transfer of a nanofluid in a vertical channel. Hatami and Khodabandeh [8] investigated the multi-slip effects on the unsteady MHD nanofluid flow and heat transfer, considering thermal radiation and convective boundary conditions. Hayat et al. [9] investigated the multi-slip effect on the stagnation point flow of Williamson nanofluid in a porous medium with Newtonian heating. Karimipour and Mirzaei [10] focused on the peristaltic motion of a Jeffrey nanofluid in an inclined channel considering the multi-slip effects. Khan et al. [11] investigated the effect of nanoparticle shape on the flow and heat transfer characteristics of a nanofluid over a stretching sheet, considering the presence of slip conditions. Khanafer and Al-Amiri [12] focused on the multi-slip effects on nanofluid flow and heat transfer in microchannels. Kole and Dey [13] investigated the slip effects on convective heat transfer of a water-based Al2O3 nanofluid flowing over a moving plate. Li et al. [14] focused on the slip and interfacial nanolayer effects on the thermophysical properties of nanofluids. Li et al. [15] investigated the thermal slip and interfacial nanolayer effect on nanofluid convective heat transfer. Mabood et al. [16] investigated the magnetohydrodynamic (MHD) mixed convection and slip flow of a nanofluid in a porous medium considering multi-slip effects. Some of the researchers ([17]-[32]) studied Multiple slip effects on nanofluid flow problems in different channels.

Motivating the above research references, the goal of this research work is to find the numerical solutions of magnetohydrodynamic Williamson-nanofluid flow towards a stretching sheet which is non-linearly filled by porous medium and in the presence of Multiple slip effects and Chemical reaction are considered. The motivation of Thermophoresis and Brownian motion effects have been considered. By using the similarity variables, a set of extremely governing partial differential equations which are non-linear are transformed into coupled linear ordinary differential equations. To achieve a

numerical solution for the flow essential governing equations, the authors have used Runge-Kutta scheme along with shooting method. The computational results for velocity, temperature, concentration, Skin-friction coefficient, Coefficients of Nusselt and Sherwood numbers are provided in graphical and tabular forms for variations of various engineering parameters. Finally, a good agreement is found between obtained results of this study and already published data. The current research has noteworthy applications in the foods industry and significance to energy systems, modern technologies in biomedical as well as aerospace engineering.

## 2. Mathematical Analysis:

In the current research work, the combined effects of Brownian motion and Thermophoresis on two-dimensional, steady, incompressible, viscous, chemically reacting, electrically conducting Williamson-nanofluid boundary layer flow towards a stretching sheet filled by porous medium in presence of Magnetic field effects are studied with the help of numerical solutions. For this examination, the fluid flow geometry is exhibited in Fig. 1. For this work, it is supposed that

i. The velocity along the x direction is $u_w(x) = ax$ (1)
ii. The stretching sheet is stretched along x-direction and y-axis is normal to it.
iii. In the domain y > 0, the Williamson-nanofluid flow is occupied.
iv. It is assumed that the convective surface temperature is $T_w$ and ambient temperature is $T_\infty$. and the concentration of the nanofluid at the sheet is $C_w$ and ambient concentration is $C_\infty$.
v. Homogeneous first order chemical reaction is considered and thermal diffusion, diffusion thermo, thermal radiation effects are neglected in this flow.
vi. Generally, B(x) a variable magnetic field will be presented to the surface of the sheet while the magnetic field induced is negligible and be justified for magnetohydrodynamic fluid flow at the small magnetic Reynolds number.

Based on the above hypotheses, the major governing equations for the conservations of mass, momentum, energy, and concentration for the Williamson-nanofluid are taken as:
Continuity Equation:

$$\left(\frac{\partial u}{\partial x}\right)+\left(\frac{\partial v}{\partial y}\right)=0 \tag{2}$$

Momentum Equation:

$$u\frac{\partial u}{\partial x}+v\frac{\partial u}{\partial y}=\nu\left(\frac{\partial^2 u}{\partial y^2}\right)+\sqrt{2}\Gamma\left[\frac{\partial u}{\partial y}\right]\left[\frac{\partial^2 u}{\partial y^2}\right]-\left(\frac{\sigma B_o^2}{\rho}\right)u-\left(\frac{\nu}{K^*}\right)u, \tag{3}$$

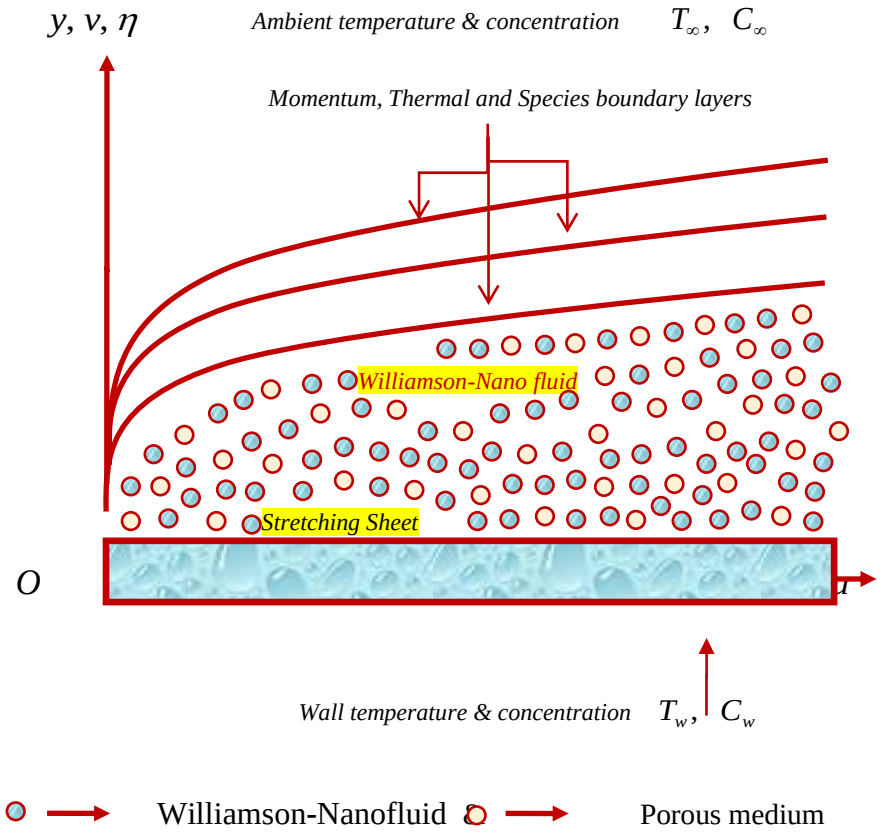


Fig. 1.: Geometry representation of the fluid

Equation of thermal energy:

$$u\frac{\partial T}{\partial x}+v\frac{\partial T}{\partial y}=\alpha\left(\frac{\partial^2 T}{\partial y^2}\right)+\tau_B\left\{D_B\left[\frac{\partial C}{\partial y}\frac{\partial T}{\partial y}\right]+\frac{D_T}{T_\infty}\left(\frac{\partial T}{\partial y}\right)^2\right\} \tag{4}$$

Equation of species nanoparticle volume concentration:

$$u\left(\frac{\partial C}{\partial x}\right)+v\left(\frac{\partial C}{\partial y}\right)=D_B\left(\frac{\partial^2 C}{\partial y^2}\right)+\frac{D_T}{T_\infty}\left(\frac{\partial^2 T}{\partial y^2}\right)-Kr\left(C-C_\infty\right) \tag{5}$$

The boundary conditions for this flow are

$$\left.\begin{aligned} &u=u_w=ax+L\left(\frac{\partial u}{\partial y}\right),\ v=0,\ T=T_w+S\left(\frac{\partial T}{\partial y}\right),\ C=C_w,\ at\ \ y=0\\ &u\to 0,\ T\to T_\infty,\ C\to C_\infty,\ as\ \ y\to\infty \end{aligned}\right\} \tag{6}$$

Introducing the following similarity transformations

$$\left.\begin{aligned} u=axf'(\eta),\ v=-\sqrt{va}\,f(\eta),\ \eta=y\sqrt{\frac{a}{v}},\ \theta=\frac{T-T_\infty}{T_w-T_\infty},\ \phi=\frac{C-C_\infty}{C_w-C_\infty},\ \psi=xf(\eta)\sqrt{av},\end{aligned}\right\} \tag{7}$$

where $\psi(x,\ y)$ represents the stream function and is defined as

$$u=\frac{\partial\psi}{\partial y}\ \text{and}\ v=-\frac{\partial\psi}{\partial x} \tag{8}$$

Making use of Eq. (7), equation of continuity is identically satisfied and Eqs. (3), (4) and (5) take the following form

$$f'''(\eta)+f(\eta).f''(\eta)-M.f'(\eta)-K.f'(\eta)-\left[f'(\eta)\right]^2+\lambda.f'''(\eta).f''(\eta)=0 \tag{9}$$

$$Le.Nb.\theta''(\eta)+\Pr.Le.Nb.f(\eta).\theta'(\eta)+\Pr.Nb.Nt.\theta'(\eta).\phi'(\eta)+\Pr.Nt.\left[\theta'(\eta)\right]^2=0 \tag{10}$$

$$Nb.\phi''(\eta)+Sc.Nb.f(\eta).\phi'(\eta)+Sc.Nt.\theta''(\eta)-Sc.\gamma.Nb.\phi(\eta)=0 \tag{11}$$

the corresponding boundary conditions (6) becomes

$$\left.\begin{array}{l} f(0)=0,\quad f'(0)=1+\beta f''(0),\quad \theta(0)=1+\delta\theta'(0),\quad \phi(0)=1 \\ \& \\ f'(\infty)\to 0,\quad \theta(\infty)\to 0,\quad \phi(\infty)\to 0 \end{array}\right\} \tag{12}$$

where the involved physical parameters are defined as

$$\left.\begin{array}{l} M=\dfrac{\sigma B_o^2}{a\rho},\ \Pr=\dfrac{\nu}{\alpha},\ Le=\dfrac{\alpha}{D_B},\ Sc=\dfrac{\nu}{D_B},\ Nb=\dfrac{(\rho C)_p D_B T_\infty (C_w-C_\infty)}{D_T(T_w-T_\infty)},\ \delta=S\sqrt{\dfrac{a}{\nu}}, \\ Nt=\dfrac{(\rho C)_p (C_w-C_\infty)}{(\rho C)_f},\ \mathrm{Re}_x=\dfrac{u_w x}{\nu},\ K=\dfrac{\nu}{aK^*},\ \lambda=\Gamma x\sqrt{\dfrac{2a^3}{\nu}},\ \gamma=\dfrac{Kr}{a},\ \beta=L\sqrt{\dfrac{a}{\nu}}, \end{array}\right\} \tag{13}$$

Measures of physical interest, the physical parameters of the skin-friction coefficient, local Nusselt number and local Sherwood number are presented as follows:

$$Cf=\frac{\tau_w}{\rho u_w^2}=\frac{\mu}{\rho u_w^2}\left(\frac{\partial u}{\partial y}+\frac{\Gamma}{\sqrt{2}}\left(\frac{\partial u}{\partial y}\right)^2\right)_{y=0}\Rightarrow\left(\sqrt{\mathrm{Re}_x}\right)Cf=f''(0)\left(1+\frac{\lambda}{2}f''(0)\right) \tag{14}$$

$$Nu_x=\frac{xq_w}{\kappa(T_w-T_\infty)}\ \text{where}\ q_w=-\kappa\left(\frac{\partial T}{\partial y}\right)_{y=0}\Rightarrow Nu=\mathrm{Re}_x^{-\frac{1}{2}}Nu_x=-\theta'(0) \tag{15}$$

$$Sh_x=\frac{xq_m}{D_B(T_w-T_\infty)}\ \text{where}\ q_m=-D_B\left(\frac{\partial C}{\partial y}\right)_{y=0}\Rightarrow Sh=\mathrm{Re}_x^{-\frac{1}{2}}Sh_x=-\phi'(0) \tag{16}$$

### 3. Numerical Solutions by Runge-Kutta Shooting Technique:

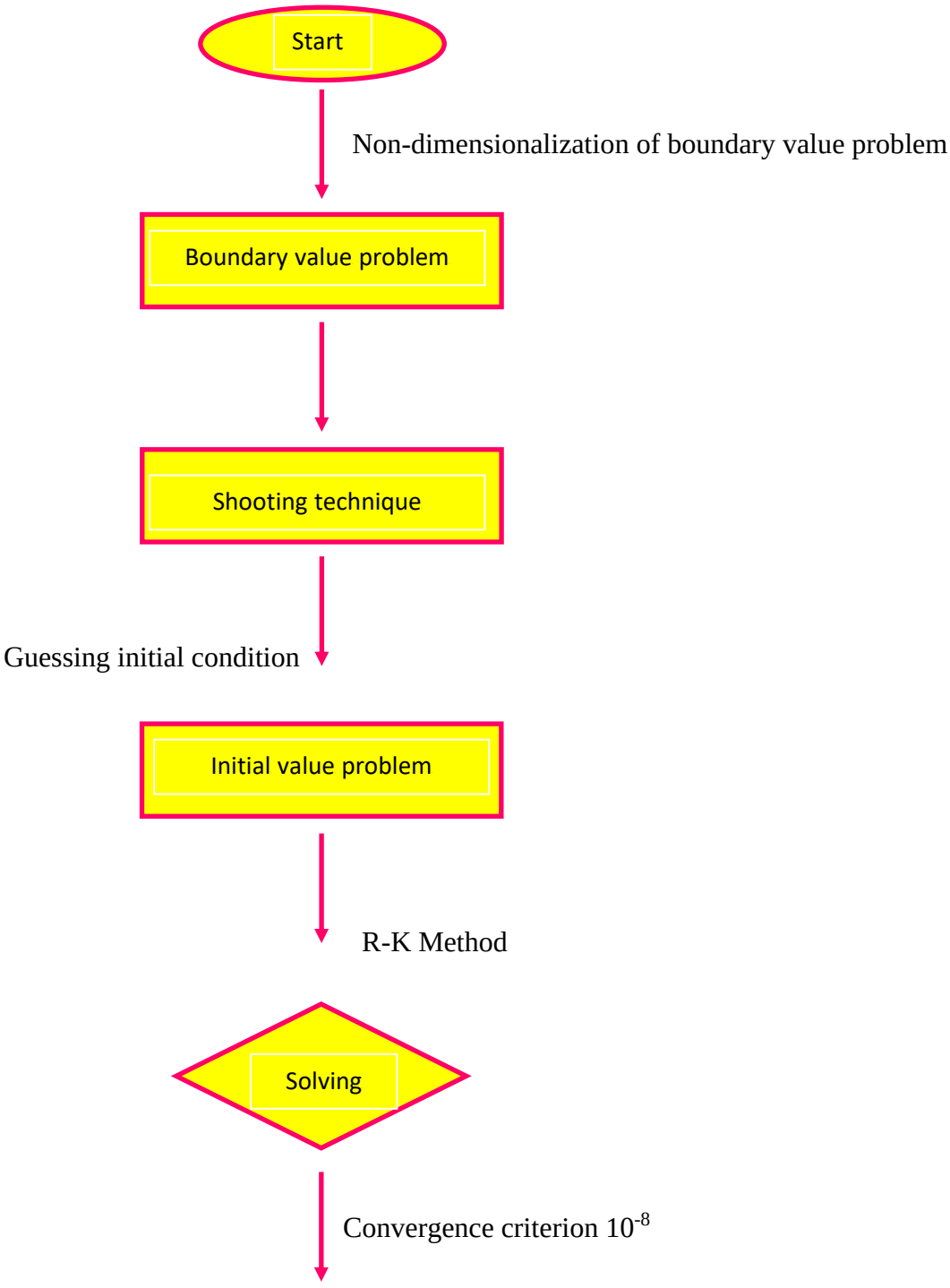


Fig. 2. Flow diagram of the numerical procedure

In order to solve the system of ordinary differential equations (9)-(11) with their corresponding initial and boundary conditions (12) numerically, the domain $[0, \infty)$ has been substituted by the bounded domain $[0, \eta_\infty]$ where $\eta_\infty$ is a suitable finite real number that should be chosen in such a way that the solution satisfies the domain. Also (9)-(11) form a highly nonlinear coupled initial

boundary value problem of third and second order ODEs. For this reason, (9)-(11) have been reduced to a system of seven initial problems of the first order of seven unknowns from the following the supposition in

$$f = y_1,\ f' = y_2,\ f'' = y_3,\ \theta = y_4,\ \theta' = y_5,\ Z = y_6,\ Z' = y_7,\ \phi = y_7,\ \phi' = y_8\} \quad (17)$$

Thus, we develop the most effective numerical technique in line with the fourth order Runge-Kutta shooting technique. The symbolic software MAPLE is used to obtain the numerical solution. To solve this system, we require seven initial conditions whereas we have only four initial conditions for $f(0)$, $f'(0)$, $\theta(0)$, and $\phi(0)$, while the other three $f''(0)$, $\theta'(0)$, and $\phi'(0)$ were not given; hence, we employ numerical shooting technique where these three initial conditions are guessed to produce the required three ending boundary conditions. During the mathematical simulation, the step size is to be $\Delta\eta$ = 0.001 in order to acquire results. The criterion of convergence is $10^{-8}$. The subsequent procedure is visualized through Fig. 2.

## 4. Program Code Validation:

Table-1: Assessment of current rate of heat transfer coefficient results with circulated results

| Pr | Khan and Pop [33] | Wang [34] | Gorla and Sidawi [35] | Present results |
|---|---|---|---|---|
| 0.07 | 0.066 | 0.066 | 0.066 | 0.586774639476943 |
| 0.20 | 0.169 | 0.169 | 0.169 | 0.157561394869386 |
| 0.70 | 0.454 | 0.454 | 0.454 | 0.436783895453409 |
| 2.00 | 0.911 | 0.911 | 0.911 | 0.893987516709311 |

To verify the correctness of computed numerical results in this work via Runge-Kutta method along with shooting technique, a comparison of numerical values of rate of heat transfer coefficient results are made for several values of Pr (Prandtl number). To do this, the achieved numerical results which are approved against the consequences of Khan and Pop [33], Wang [34] and Golra and Sidawi [35] as presented in table-1. It is observed that numerical results of present analysis are found in good agreement.

## 5. Results and Discussion:

A mathematical modelling is presented to investigate the effects of Multiple slip effects on Williamson-Nanofluid flow through a stretching sheet surrounded by porous medium with the influence of Magnetic field, Chemical reaction, Thermophoresis and Brownian motion using Runge-Kutta method along with shooting technique solutions. The behaviours of various emerging parameters Magnetic field (M), Permeability parameter (K), Williamson fluid parameter (λ), Velocity slip parameter (β), Prandtl number (Pr), Thermophoresis parameter (Nt), Brownian motion parameter (Nb), Lewis number (Le), Thermal slip parameter (δ), Schmidt number (Sc) and Chemical reaction parameter (γ) on velocity, temperature and concentration profiles are discussed and presented in Fig. 3, Fig. 4, Fig. 5, Fig. 6, Fig. 7, Fig. 8, Fig. 9, Fig. 10, Fig. 11, Fig. 12, Fig. 13, Fig. 14, Fig. 15. Also,

the numerical values of Skin-friction coefficient, Rate of heat transfer coefficient (Nusselt number) and Rate of mass transfer coefficient (Sherwood number) are presented in Table-2, Table-3 and Table-4. For this investigation the basic values of all parameters are fixed as: M = 0.5, K = 0.5, $\lambda$ = 0.5, $\beta$ = 0.5, Pr = 0.71, Nb = 0.3, Nt = 0.1, Le = 0.5, Sc = 0.22, $\delta$ = 0.5 and $\gamma$ = 0.5.

- Fig. 3 illustrates the connection in velocity for magnetic field parameter (M) values. The rise in M has been shown to reduce velocity. As M elevates, a resistive force similar to a drag force is generated, which is known as Lorentz force. The velocity intensity is retarded by the Lorentz force, which decelerates its motion.
- The graph in Fig. 4 shows that the fluid-flow resistive force decreases with the rise in the porosity parameter or permeability parameter (K), i.e. when the porosity parameter increases, resulting in increased velocity of fluid-flow.
- In Fig. 5, the effect of the Williamson fluid parameter ($\lambda$) on the velocity profiles, and it clears that this effect is negative in the sense that the increase in the values of this coefficient is followed by a decrease in velocity of the fluid, which makes its movement slow.
- Fig. 6 shows the effects of velocity slip parameter ($\beta$) on stream wise velocity of the fluid. Relative velocity of the stretching sheet and fluid declines with increase in velocity slip parameter. This is due to the fact that nanofluid velocity is decreasing function of velocity slip parameter.
- The variability in temperature profiles is shown by the Prandtl number Pr, which can be found by Fig. 7. It has been observed that when Pr values go down, temperature profiles go down with them. This is because the fluid has a lower Prandtl number, which leads to less thermal diffusivity and a higher heat transfer rate. As a consequence of this, the fluid has a lower thermal diffusivity. Fluids with a lower Prandtl number Pr have a greater thermal conductivity, which leads in thicker thermal boundary layer structures than fluids with a higher Prandtl number Pr. This is due to the fact that lower Prandtl numbers correspond to higher thermal conductivities.
- Figs. 8 and 9 have been drawn with the intention of demonstrating the behaviour of the Brownian motion parameter, denoted by the symbol Nb, on dimensionless temperature and concentration curves. As the Nb values increase, the concentration profiles go lower, while the temperature profiles get higher. Rising values of the Brownian motion parameter magnify chaotic motion, which increases the kinetic energy of the nanoparticles and, as a result, the temperature of the nanofluid. This is because the definition of Brownian motion states that chaotic motion increases.
- The influence that the thermophoresis parameter Nt has on the temperature and concentration curves is seen in figures 10 and 11. The values of the thermophoresis parameter increase, which results in an increase in both the temperature and concentration profiles. In addition to that, the thickness of the border layer increases. This happens on a more fundamental level because of a phenomenon known as thermophoresis, which is triggered when there is a significant temperature difference between the sheet and the fluid.
- From Fig. 12 it is observed that the temperature as well as thermal boundary layer thickness decreases, with increase in Lewis number (Le).
- Fig. 13 illustrates the influence of Schmidt number (Sc) on dimensionless concentration profiles. As the Schmidt number Sc grows higher, it is observed that concentration decreases.

- In Fig. 14, the impact of the chemical reaction (γ) on the concentration profile is shown. As the chemical reaction goes up, it is witnessed that concentration decreases.
- Fig. 15 exhibit the effect of the thermal slip parameter (δ) on the dimensionless temperature profiles. It is clearly shown that by increasing the values of δ, the temperature profiles are decreases. As the value of the thermal slip parameter increases, the thermal boundary layer thickness decreases even when a small amount of heat is transferred to the fluid from the sheet.
- Table-2 shows the numerical data of Skin-friction ( f′ (0)(1+(λ/2) f′ (0)) coefficient for changes of M, K, λ, Pr, Le, Nb, Nt, β, δ, Sc and γ. From this table, the Skin-friction ( f′ (0)(1+(λ/2) f′ (0)) coefficient is increasing with increasing values of Nb, Nt, while it is decreasing with increasing values of M, K, λ, Pr, Le, β, δ, Sc and γ.

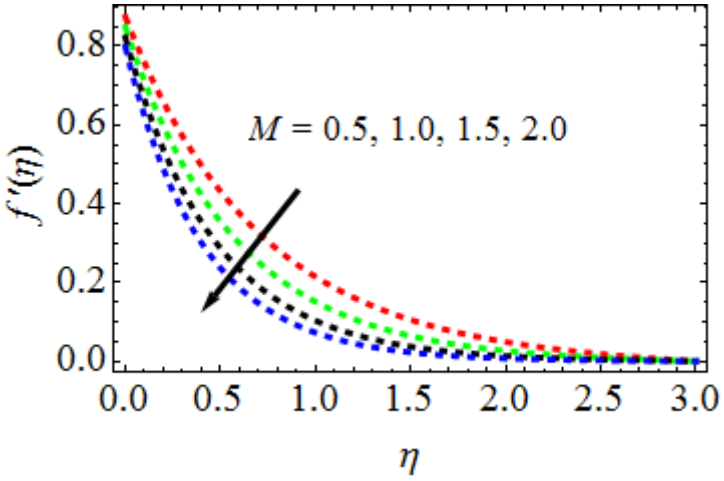


Fig. 3. M behaviour on velocity profiles

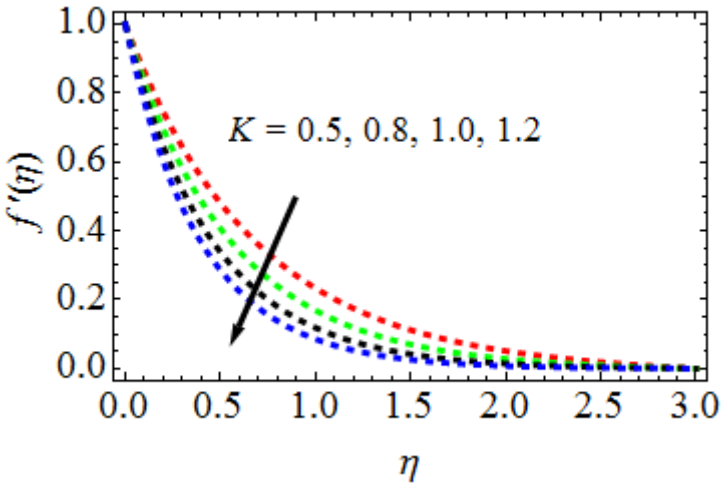


Fig. 4. K behaviour on velocity profiles

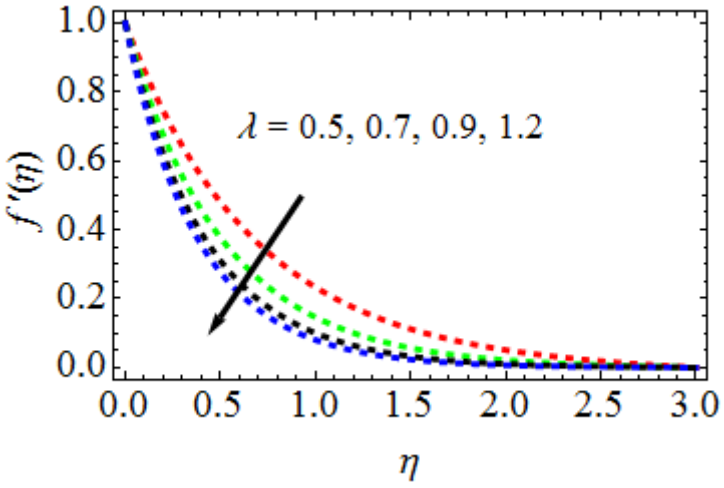


Fig. 5. λ behaviour on velocity profiles

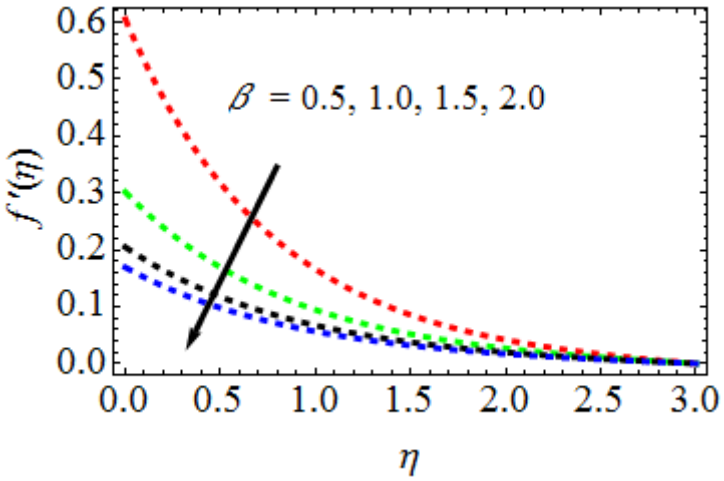


Fig. 6. β behaviour on velocity profiles

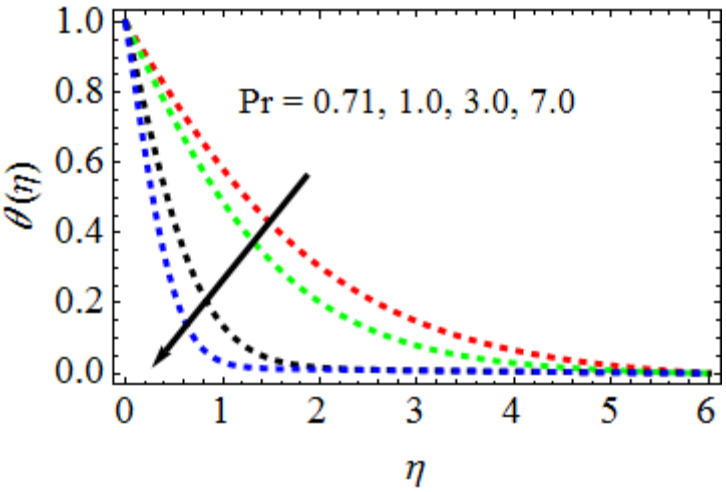


Fig. 7. Pr behaviour on temperature profiles

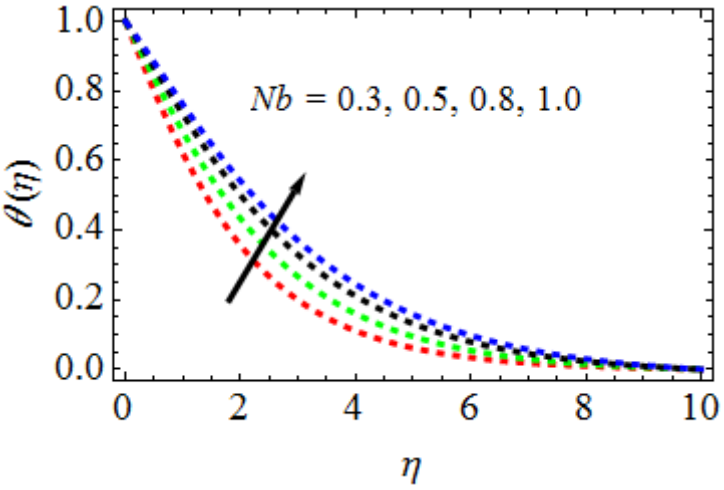


Fig. 8. Nb behaviour on temperature profiles

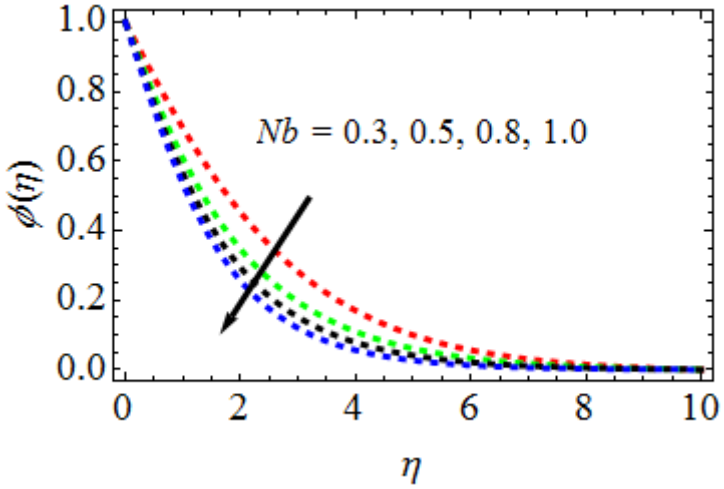


Fig. 9. Nb behaviour on concentration profiles

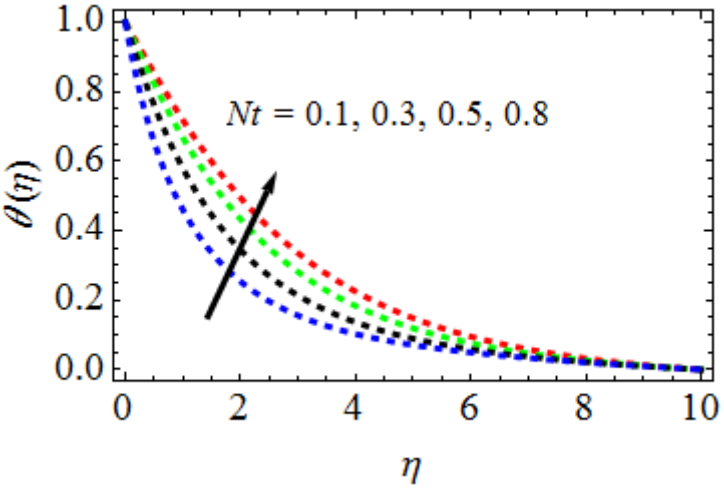


Fig. 10. Nt behaviour on temperature profiles

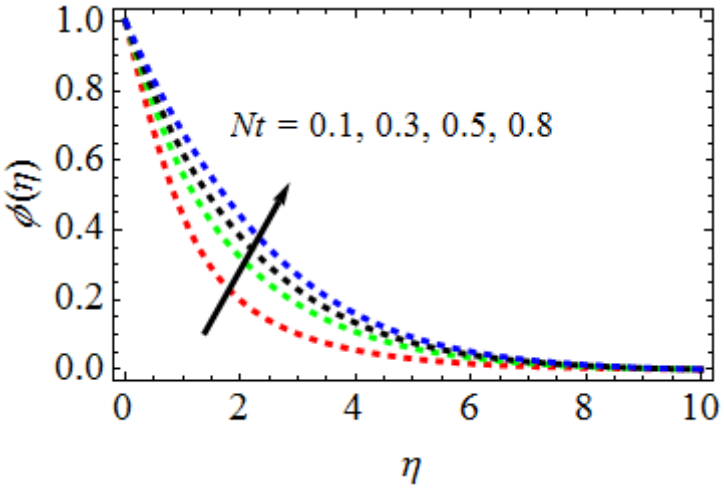


Fig. 11. Nt behaviour on concentration profiles

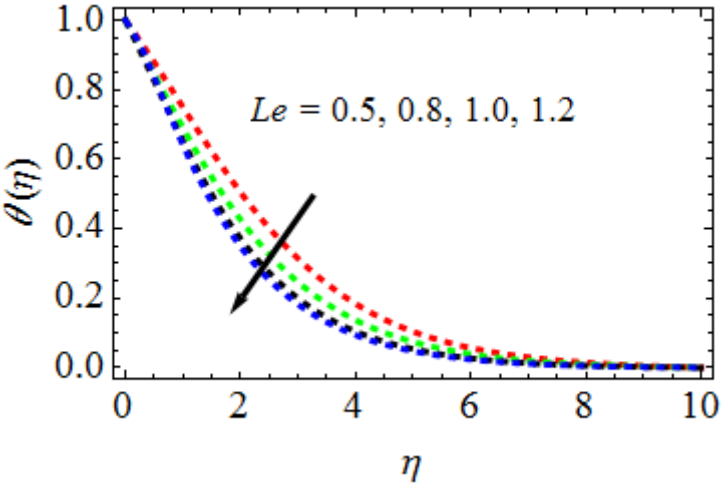


Fig. 12. Le behaviour on temperature profiles

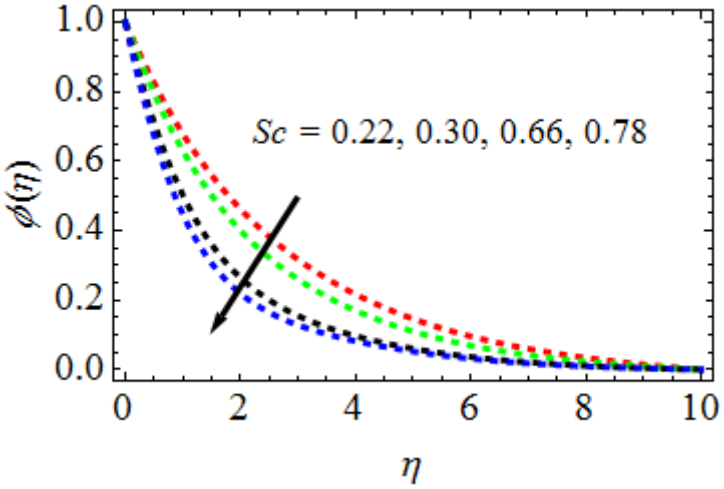


Fig. 13. Sc behaviour on concentration profiles

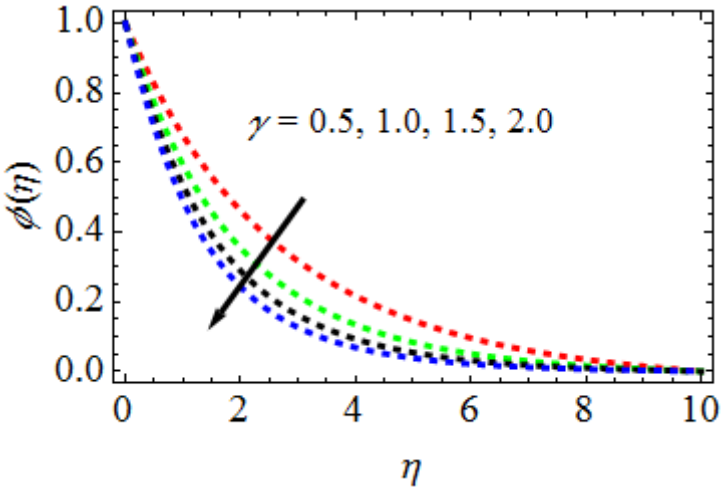


Fig. 14. γ behaviour on concentration profiles

Table-2: Numerical values of Skin-friction coefficient for different values of M, K, λ, Pr, Le, Nb, Nt, β, δ, Sc and γ

| *M* | *K* | *λ* | Pr | *Le* | *Nb* | *Nt* | *β* | *δ* | *Sc* | *γ* | $f''(0)(1+(\lambda/2)f''(0)$ |
|---|---|---|---|---|---|---|---|---|---|---|---|
| 0.5 | 0.5 | 0.5 | 0.71 | 0.5 | 0.3 | 0.1 | 0.5 | 0.5 | 0.22 | 0.5 | 1.476639836983913 |
| **1.0** | | | | | | | | | | | 1.446876790867309 |
| **1.5** | | | | | | | | | | | 1.411789869837646 |
| | **0.8** | | | | | | | | | | 1.456769138763904 |
| | **1.0** | | | | | | | | | | 1.431675380610375 |
| | | **0.7** | | | | | | | | | 1.446679876512981 |
| | | **0.9** | | | | | | | | | 1.425671075609756 |
| | | | **1.00** | | | | | | | | 1.457888778713872 |
| | | | **3.00** | | | | | | | | 1.437686789798266 |
| | | | | **0.8** | | | | | | | 1.459798657238082 |
| | | | | **1.0** | | | | | | | 1.436782909867239 |
| | | | | | **0.5** | | | | | | 1.490813689634663 |
| | | | | | **0.8** | | | | | | 1.517856874684678 |
| | | | | | | **0.3** | | | | | 1.506767806176371 |
| | | | | | | **0.5** | | | | | 1.529876137609316 |
| | | | | | | | **1.0** | | | | 1.459769136364099 |
| | | | | | | | **1.5** | | | | 1.438998079872140 |
| | | | | | | | | **1.0** | | | 1.448798173498734 |
| | | | | | | | | **1.5** | | | 1.423467691843993 |
| | | | | | | | | | **0.30** | | 1.439716283761846 |
| | | | | | | | | | **0.66** | | 1.408578919834839 |
| | | | | | | | | | | **1.0** | 1.447863418763847 |
| | | | | | | | | | | **1.5** | 1.426787601396003 |

- The numerical results of rate of heat transfer (- θ′ (0)) in terms of Nusselt number for different values of Pr, Le, Nb, Nt, and δ, are presented in Table-3. From this table, it is observed that, the

heat transfer rate is rising with growing values of Nb, Nt, while it reducing for increasing values of δ, Pr and Le.

- Rate of mass transfer (- ϕ′ (0)) in terms of Sherwood number for variations of Nb, Nt, Sc and γ are presented in Table-4. From this table, it is noticed that Sherwood number (- ϕ′ (0)) is growing with higher values of Nt, and the reverse effects is observed in case of increasing values of Sc, Nb and γ.

Table-3: Numerical values of Nusselt number coefficient for different values of Pr, Le, Nb, Nt and δ

| Pr | Le | Nb | Nt | δ | Nu |
|---|---|---|---|---|---|
| 0.71 | 0.5 | 0.3 | 0.1 | 0.5 | 0.686579974659374 |
| 1.00 | | | | | 0.659765176740838 |
| 3.00 | | | | | 0.621586598556282 |
| | 0.8 | | | | 0.655687106878170 |
| | 1.0 | | | | 0.624818750875784 |
| | | 0.5 | | | 0.707678716439033 |
| | | 0.8 | | | 0.726786791839679 |
| | | | 0.3 | | 0.719667834673496 |
| | | | 0.5 | | 0.739461783476034 |
| | | | | 1.0 | 0.669677346373873 |
| | | | | 1.5 | 0.641578638753829 |

Table-4: Numerical values of Sherwood number coefficient for different values of Nb, Nt, Sc and γ

| Nb | Nt | Sc | γ | Sh |
|---|---|---|---|---|
| 0.3 | 0.1 | 0.22 | 0.5 | 0.985674697459442 |
| 0.5 | | | | 0.955671085620871 |
| 0.8 | | | | 0.938657532578282 |
| | 0.3 | | | 1.056576487068094 |
| | 0.5 | | | 1.080910197679277 |
| | | 0.30 | | 0.959776186287270 |
| | | 0.66 | | 0.938747845618745 |
| | | | 1.0 | 0.957897987983381 |
| | | | 1.5 | 0.927565265326366 |

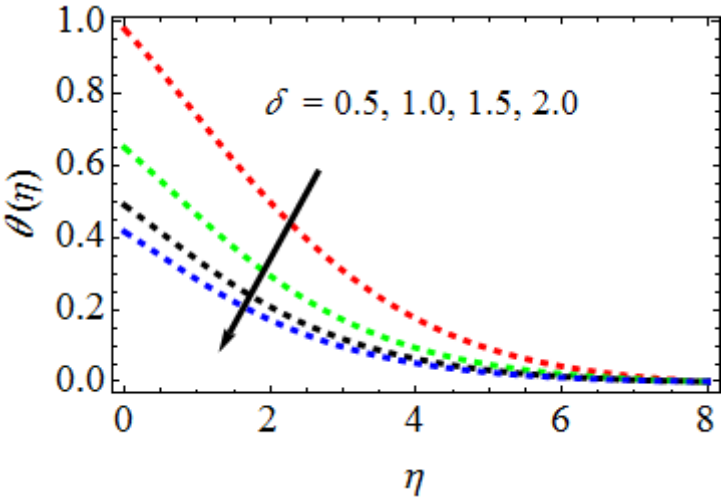


Fig. 15. δ behaviour on temperature profiles

## 6. Conclusions:

Investigations for MHD of Williamson fluid with nanofluid flow through a stretching sheet filled by porous medium have been carried out under the impacts of Chemical reaction, Brownian motion, Multiple slips and Thermophoresis. The governing partial differential equations for mass, momentum, energy and concentration are turned into ordinary differential equations with the help of similar transformations. In this work, the numerical solutions are obtained under the thermal and velocity slip boundary conditions with the help of Runge-Kutta method along with shooting technique. Using the numerical solutions, 2-D plots of velocity, temperature and concentration profiles are drawn based on the combined effects of various engineering parameters. In conclusion of this work, key findings are given below:

- A rising value in the M, as a consequence, diminishes the dimensionless velocity.
- The velocity profiles falls down for variations of Williamson fluid parameter λ.
- The velocity profiles decrease with rising values of velocity slip parameter β.
- Permeability parameter K increases, a decrease in velocity profiles.
- With an enhanced in Prandtl number Pr, the temperature profiles is diminished.
- An increase in the temperature, decreases in the thermal slip parameter δ.
- The larger values of the Schmidt number Sc and the Chemical reaction parameter γ serve to diminishes the profiles of concentration.
- Mass transfer rate increases for the larger values of Thermophoresis parameter.
- This investigation has many applications in chemical engineering and aerospace Engineering.

## References:

[1] Ahmadi, G., Behzadmehr, A., & Ghasemi, R. (2009). Modeling of Laminar Forced Convection of a Nanofluid in a Tube with Uniform Heat Flux Using Buongiorno's Mathematical Model. Journal of Heat Transfer, 131(2), 023503. doi:10.1115/1.3056595

[2] Ali, H. M., Rashidi, M. M., & Lorenzini, G. (2020). A comprehensive review of the thermal slip phenomenon and its implications on the performance of nanofluid-based systems. International Journal of Heat and Mass Transfer, 158, 119973.
[3] Aswathy, R. G., & Philip, J. (2019). Slip velocity models for nanofluids: A review. Journal of Molecular Liquids, 284, 1-14.
[4] Aswathy, R. G., & Philip, J. (2021). Multi slip effect in nanofluid flow: A review. Journal of Molecular Liquids, 325, 115086.
[5] Bhanvase, B. A., & Chhabra, R. P. (2020). Slip flow heat transfer of nanofluids in microchannels. Nanofluid Heat and Mass Transfer in Engineering Problems, 19-39.
[6] Chein, R. Y., Hsu, W. W., & Chen, C. K. (2013). Viscous Dissipation and Non-Newtonian Slip Effects on the Mixed Convection of Williamson Nanofluid Flow through a Vertical Wavy Channel. International Communications in Heat and Mass Transfer, 48, 116-121. doi:10.1016/j.icheatmasstransfer.2013.08.002
[7] Ghosh, S., & Das, P. K. (2014). Multi-Slip Effects on Mixed Convection Flow and Heat Transfer of a Nanofluid in a Vertical Channel. Journal of Heat Transfer, 136(2), 022502. doi: 10.1115/1.4025783
[8] Hatami, M., & Khodabandeh, R. (2017). Multi-slip effect on unsteady MHD nanofluid flow and heat transfer considering thermal radiation and convective boundary conditions. Journal of Molecular Liquids, 241, 1094-1107.
[9] Hayat, T., Zaman, G., Iftikhar, A., Alsaedi, A., & Ahmed, B. (2020). Multi slip effect on stagnation point flow of Williamson nanofluid in a porous medium with Newtonian heating. Journal of Molecular Liquids, 303, 112617.
[10] Karimipour, A., & Mirzaei, M. (2017). Multi-slip effects on the peristaltic motion of a Jeffrey nanofluid in an inclined channel. Journal of Molecular Liquids, 238, 228-236.
[11] Khan, W. A., Pop, I., & Ali, M. E. (2019). The effect of nanoparticle shape on the flow and heat transfer of a nanofluid over a stretching sheet in the presence of slip conditions. International Journal of Heat and Mass Transfer, 133, 957-967.
[12] Khanafer, K., & Al-Amiri, A. (2017). Multi-Slip Effects on Nanofluid Flow and Heat Transfer in Microchannels. Nanoscience and Nanotechnology Letters, 9(12), 2105-2113. doi: 10.1166/nnl.2017.2497
[13] Kole, M., & Dey, T. K. (2013). Slip effects on convective heat transfer of water-based Al2O3 nanofluid flow over a moving plate. International Journal of Heat and Mass Transfer, 57(1), 110-118.
[14] Li, Z., Li, C., Zhou, J., Wang, L., & Wu, J. (2018). Slip and interfacial nanolayer effects on the thermophysical properties of nanofluids. International Journal of Heat and Mass Transfer, 121, 115-124.
[15] Li, Z., Zhou, J., Guo, K., He, Y., Li, C., & Wang, L. (2017). Investigation of thermal slip and interfacial nanolayer effect on nanofluid convective heat transfer. International Journal of Heat and Mass Transfer, 105, 86-94.
[16] Mabood, F., Khan, W. A., & Ismail, A. I. (2017). MHD mixed convection and slip flow of a nanofluid in a porous medium with multi-slip effects. International Journal of Heat and Mass Transfer, 104, 951-959.
[17] Mahian, O., Kianifar, A., Sahin, A. Z., Wongwises, S., & Yasinsky, V. (2013). Slip flow and heat transfer in a microchannel heat sink with nanofluids. International Journal of Heat and Mass Transfer, 61, 423-431.
[18] Nield, D. A., & Kuznetsov, A. V. (2010). Slip Effects in Forced Convection from a Porous Flat Plate with a Uniform Surface Heat Flux. International Journal of Heat and Mass Transfer, 53(11-12), 2267-2275. doi:10.1016/j.ijheatmasstransfer.2010.02.001
[19] Rana, P., & Bhargava, R. (2017). Thermal radiation and slip effects on MHD flow of Williamson nanofluid over a permeable stretching sheet: A numerical study. Journal of Molecular Liquids, 229, 160-168.
[20] Rashidi, M. M., & Esfahani, J. A. (2015). Multi slip effects on MHD mixed convection of a nanofluid in a vertical microchannel. International Journal of Heat and Mass Transfer, 87, 535-542.
[21] Sajjadi, H., & Taeibi-Rahni, M. (2015). The effects of Brownian motion, thermophoresis, and slip boundary condition on the natural convection in a nanofluid-filled cavity using the two-phase mixture model. International Journal of Heat and Mass Transfer, 81, 473-487.
[22] Sankar, R., & Sivasankaran, S. (2018). Heat and mass transfer characteristics of a Williamson nanofluid over a stretching sheet with suction/injection, slip and thermal radiation. Journal of Molecular Liquids, 253, 250-261.
[23] Sharma, R. K., & Bhargava, R. (2015). Multi Slip Effects on MHD Nanofluid Flow and Heat Transfer. Journal of Nanofluids, 4(2), 198-207.
[24] Sheikholeslami, M., & Rokni, H. B. (2019). Numerical modeling of multi-slip effects on Al2O3–water nanofluid flow in a porous medium. Journal of Thermal Analysis and Calorimetry, 135(1), 449-460.

[25] Sheikholeslami, M., Rokni, H. B., Rashidi, M. M., & Thongchattu, W. (2019). Multi-slip effects on mixed convection of water-based nanofluid in a channel with sinusoidal temperature distribution. International Journal of Heat and Mass Transfer, 129, 527-535.
[26] Singh, A., & Kumar, R. (2016). Analytical study of multi-slip effects on magnetohydrodynamic nanofluid flow and heat transfer characteristics. International Journal of Heat and Mass Transfer, 93, 44-53.
[27] Singh, A., Kumar, R., & Jang, S. P. (2014). Multi slip effects on magnetohydrodynamic nanofluid flow and heat transfer characteristics: A review. International Journal of Heat and Mass Transfer, 78, 219-233.
[28] Sundar, L. S., Singh, M. K., & Vaidyanathan, S. (2017). A Review on Slip Models for Flow of Nanofluids and Nanolubricants. Nanoscale and Microscale Thermophysical Engineering, 21(4), 227-253. doi:10.1080/15567265.2017.1340640
[29] Uddin, M. J., Khan, M. M., Ismail, A. I., & Al-Mdallal, Q. M. (2018). Nonlinear mixed convection slip flow and heat transfer of a nanofluid with multi slip effects past a permeable wedge. Journal of Molecular Liquids, 256, 146-156.
[30] Wang, L., Li, Z., Zhou, J., & Zhang, J. (2019). Slip flow and heat transfer of nanofluids in microchannels: A review. International Journal of Heat and Mass Transfer, 134, 751-762.
[31] Zeng, J., Wang, W., & Mujumdar, A. S. (2019). Thermal, solutal, and hydrodynamic slip effects on nanofluid flow and heat transfer: A review. International Journal of Thermal Sciences, 135, 267-280.
[32] Zhang, X., & Fu, X. (2018). A review on multi-slip effects in nanofluids: Theories, models, and applications. International Journal of Heat and Mass Transfer, 124, 1322-1342.
[33] Khan, W. A., Pop, I., (2010). Boundary-layer flow of a nanofluid past a stretching sheet. Int. J. Heat Mass Transf., 53, 2477-2483.
[34] Wang, Y., (1989). Free convection on a vertical stretching surface. J. Appl. Math. Mech., 69, 418-420.
[35] Gorla, R. S. R., Sidawi, I., (1994). Free convection on a vertical stretching surface with suction and blowing. Appl. Sci. Res., 52, 247-257.